Slip Distributions of Short-Term Slow Slip Events in Shikoku, Southwest Japan, From 2001 to 2019 Based on Tilt Change Measurements

Hirose, Hitoshi

Kimura, Takeshi

(Citation)
Journal of Geophysical Research. Solid Earth,125(6):e2020JB019601-e2020JB019601

(Issue Date)
2020-06

(Resource Type)
journal article

(Version)
Version of Record

JGR Solid Earth

RESEARCH ARTICLE
10.1029/2020JB019601

Special Section:
Creep on Continental Faults and Subduction Zones: Geophysics, Geology, and Mechanics

Slip Distributions of Short-Term Slow Slip Events in Shikoku, Southwest Japan, From 2001 to 2019 Based on Tilt Change Measurements

Hitoshi Hirose[1,2,3] and **Takeshi Kimura**[3]

[1]Research Center for Urban Safety and Security, Kobe University, Kobe, Japan, [2]Department of Planetology, Kobe University, Kobe, Japan, [3]National Research Institute for Earth Science and Disaster Resilience, Tsukuba, Japan

Key Points:
- The slip distributions of 61 short-term slow slip events (SSEs) from 2001 to 2019 in Shikoku, Japan, are estimated from tilt offset data
- The estimated slip history of the SSEs shows that the SSE zone is divided into three segments
- The number of short-term SSEs with larger slip extent and seismic moment increases after 2012

Supporting Information:
- Supporting Information S1
- Figure S1
- Movie S1

Correspondence to:
H. Hirose,
hitoshi.hirose@ruby.kobe-u.ac.jp

Citation:
Hirose, H., & Kimura, T. (2020). Slip distributions of short-term slow slip events in Shikoku, southwest Japan, from 2001 to 2019 based on tilt change measurements. *Journal of Geophysical Research: Solid Earth*, *125*, e2020JB019601. https://doi.org/10.1029/2020JB019601

Received 15 FEB 2020
Accepted 18 MAY 2020
Accepted article online 26 MAY 2020

Abstract In the southwest Japan subduction zone, short-term slow slip events (SSEs) accompanying nonvolcanic tremor (ETS: episodic tremor and slip) occur repeatedly with recurrence intervals of several months. It is important to know the detailed slip areas of the SSEs because short-term SSEs occur at the downdip extension of a megathrust earthquake rupture zone, and hence, the SSEs play a key role in the stress buildup processes of the megathrust earthquakes. Although most of the previous studies model a SSE fault motion with uniform slip on a rectangular fault, this may lead to a bias in estimating the slip area. In this study we estimate a spatial slip distribution for each of the short-term SSEs from tilt offset measurements. In total, the slip distributions of 61 SSEs in Shikoku from January 2001 to March 2019 are obtained. The ETS zone in Shikoku is divided into three segments in terms of slip history of the SSEs. Before 2011, the slip areas of most of the SSEs are limited in any one of the three segments. After 2012, however, the number of SSEs having a slip area that extends to multiple segments increases. The slip histories at each position in the ETS zone suggest that the short-term SSE activity is affected by the occurrence of nearby long-term SSEs. The average slip rate over 18 years suggests that an estimated slip deficit in the ETS zone in western Shikoku could be released by long-term SSEs, or coseismic slip or afterslip of the megathrust earthquakes.

1. Introduction

The Nankai trough subduction zone in southwest Japan hosts a variety of slip events from megathrust earthquakes to slow earthquakes associated with the subduction of the Philippine Sea plate (e.g., Obara & Kato, 2016). Along the subducting plate interface around the Shikoku area (Figure 1), megathrust earthquakes of magnitude 8 class recur every 100 to 200 years at a shallower depth off Shikoku (e.g., Ando, 1975; Sagiya & Thatcher, 1999) and large but smaller earthquakes (magnitude 7 class) occur more frequently off the east coast of Kyushu (e.g., Yagi et al., 1998). At the deeper extension of the plate interface, short-term slow slip events (SSEs) with a typical duration of approximately 1 week accompanying tremor activities (Obara, 2002), called episodic tremor and slip (ETS; Rogers & Dragert, 2003), repeatedly occur with recurrence intervals of a few to several months (e.g., Hirose & Obara, 2005; Obara et al., 2004; Sekine et al., 2010). Between the shallower seismogenic zone and the deeper ETS zone, SSEs of much longer duration (months to years), called long-term SSEs, recur with several-year intervals (Hirose et al., 1999; Kobayashi, 2010, 2012, 2017; Takagi et al., 2019; Yarai & Ozawa, 2013). Among these slip phenomena, it is important to know the characteristics of the ETS activity because the ETS occurs most frequently, the ETS acts as a stress loading process of the megathrust rupture (e.g., Mazzotti & Adams, 2004), and hence this is a key to understanding a current stress level of the megathrust source area.

Another important feature of the ETS activity for constraining a possible rupture extent of a future megathrust earthquake is the strain budget accumulated by a relative plate convergence and released by short-term SSEs. This is because a megathrust rupture front might be prevented from propagating into the ETS zone if the accumulated strain is nearly 0 at the ETS zone when a megathrust earthquake occurs. In order to assess the strain budget in the ETS zone, a number of fault models of recurrent short-term SSEs for several years in a particular area have been estimated based on geodetic observations. For example, Sekine et al. (2010) reported from tiltmeter data that approximately 65% of the accumulated moment by the relative plate convergence is released as short-term SSEs in the western Shikoku area. Nishimura et al. (2013) also show that

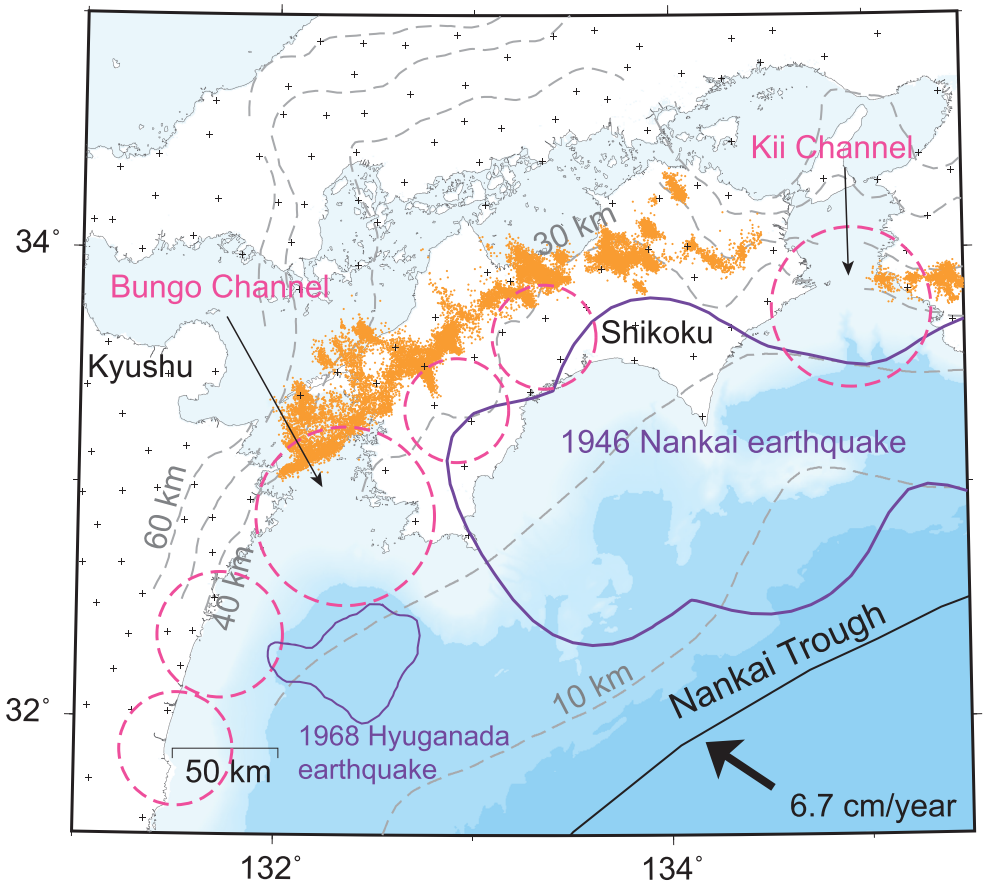

Figure 1. Index map showing the tectonic settings of the study area. The black solid line shows the Nankai Trough axis. The gray dashed lines indicate the depth of the subducting Philippine Sea plate (Baba et al., 2006; Shiomi et al., 2008). The purple contours show the source areas of the 1946 Nankai earthquake (Sagiya & Thatcher, 1999) and 1968 Hyuganada earthquake (Yagi et al., 1998). The magenta dashed circles denote the source areas of long-term SSEs (Hirose et al., 1999; Kobayashi, 2010, 2012; Takagi et al., 2019; Yarai & Ozawa, 2013). The orange dots show the epicenters of tremors (Obara et al., 2010). Crosses represent the NIED Hi-net locations.

the cumulative slip of the short-term SSEs in western Shikoku is, at most, only about half of the relative plate motion from a Global Navigation Satellite System (GNSS) data analysis. These estimations are based on a fault model such that slip is uniform on a plane rectangular fault and that an SSE fault is modeled as a rectangle fault. This may lead to a bias in the estimation of the fault area and slip of an SSE.

An effective way to avoid such a bias is to use a model that is able to express a spatial slip distribution. Hirose and Obara (2010) applied a network inversion filter (NIF) technique (Segall & Matthews, 1997) to tilt time series data and estimated the spatial and temporal slip evolutions of several short-term SSEs in western Shikoku. Their method is a powerful tool when high-quality tilt time series records are available at several stations. However, this is not always the case. Indeed, this method is not applicable to data sets of a number of short-term SSE episodes in which rectangular fault models are obtained (Hirose & Obara, 2010). It is crucial to obtain as complete a catalog of the slip distributions of the SSEs as possible in order to discuss the strain budget in the ETS zone.

Therefore, we apply an inversion method that can express a spatial fault slip distribution but does not use information on temporal variation to tilt offset data in Shikoku that are measured in previous studies (e.g., Hirose & Obara, 2005; Sekine et al., 2010) in order to obtain a more complete set of slip distributions of the short-term SSEs from January 2001 to March 2019. We also discuss the temporal change in the activity of the short-term SSEs for 18 years based on this catalog.

2. Data

The National Research Institute for Earth Science and Disaster Resilience (NIED) operates a high-sensitivity seismograph network Japan (Hi-net). The Hi-net station locations are shown in Figure 1. At each Hi-net station, a tiltmeter is equipped with a high-sensitivity short-period seismograph and a strong-motion seismograph (accelerometer) at the bottom of a borehole (Obara et al., 2005; Okada et al., 2004). The tiltmeters have been used to detect tilt deformations caused by short-term SSEs (e.g., Hirose & Obara, 2005; Obara et al., 2004). In this study, we use a NIED tilt offset data set, which is a set of tilt measurements of the short-term SSEs (e.g., Hirose & Obara, 2005; Sekine et al., 2010) from January 2001 to March 2019. The data set and a full list of references for each of the tilt offset measurements can be obtained from an NIED repository (see Data Availability Statement).

Typical tilt data processing for this data set is as follows. At first, a transient signal possibly associated with an SSE is identified from a time series plot of tiltmeter records with tremor activity, atmospheric pressure, and rainfall. This includes the determination of an event period, that is, event duration. Next, records that contain large disturbances likely caused by rainfall and/or unidentified origin are rejected. After this station selection process, a tilt offset is measured as the difference between the averages of tilts in two 1-day-long time intervals just before and after an SSE episode (the length of the averaging time interval can vary on a case-by-case basis) after a preprocessing, such as removal of tidal components, an atmospheric pressure response correction, and removal of a linear trend (Hirose & Obara, 2005) (examples of the preprocessed tilt time series are shown in Figure S1 in the supporting information). At the same time, the standard deviation of the same time intervals, which is used for weighting data in the inversion, is also calculated. In total, tilt offset data at 30 stations of 61 short-term SSE episodes in Shikoku are analyzed.

Note that we considered a time period in which a tilt transient is spatiotemporally continuous as "an event period" in this study. Although a series of tilt transients separated by a short time interval is considered as a single event in some studies (e.g., Event IDs 201112 and 201201 in this study; NIED, 2012), we consider these events to be separate. On the other hand, previous studies sometimes divide a tilt transient episode into several stages in order to discuss the time development of tilt deformations and slip. In this case, we add all of the observed tilt changes in the transient at each station and will obtain a final slip distribution for the slip episode (e.g., August 2003 episode in Hirose & Obara, 2005 and 200308 in this study).

We use the NIED tremor catalog for comparison with an obtained slip distribution of an SSE. This catalog is generated by applying a detection and location method by Maeda and Obara (2009) and a clustering procedure developed by Obara et al. (2010) to continuous waveform data obtained using the NIED Hi-net short-period seismographs. This catalog can be obtained from the Hi-net web page (http://www.hinet.bosai.go.jp/?LANG=en).

3. Methods

In order to invert a set of tilt offset measurements, we apply a conventional slip inversion method to the data set. A slip distribution is modeled by a superposition of 21 × 5 basis functions with a spacing of 10 km in Shikoku (Figure 2). Each basis function is expressed by 11 × 11 smaller rectangular faults (the area of a fault is ~2 × 2 km^2) placed on the plate interface geometry of the subducting Philippine Sea plate constructed based on Shiomi et al. (2008) and Baba et al. (2006) (Figure 1). We use a linear B-spline function as the basis function. Synthetic tilt deformations due to slip on a rectangular fault in a homogeneous elastic half-space are computed based on Okada (1992). A rigidity of 40 GPa is assumed. The slip direction is fixed to a relative plate convergence direction (Miyazaki & Heki, 2001).

The observation equation is expressed as

$$\mathbf{d} = \mathrm{H}\mathbf{m}, \tag{1}$$

where $\mathbf{d}$ is a data vector, H is a design matrix, and $\mathbf{m}$ is a model vector that consists of slip at the center of each basis function (the center position is hereinafter referred to as a knot). The number of components in $\mathbf{m}$, that is, the number of basis functions is expressed as M. The data vector $\mathbf{d}$ is as follows:

$$\mathbf{d} = \left[t_{\mathrm{E}}^{1}, t_{\mathrm{N}}^{1}, t_{\mathrm{E}}^{2}, t_{\mathrm{N}}^{2}, \ \cdots \ , t_{\mathrm{E}}^{N_{\mathrm{sta}}}, t_{\mathrm{N}}^{N_{\mathrm{sta}}}, 0, \ \cdots \ , 0\right]^{T}, \tag{2}$$

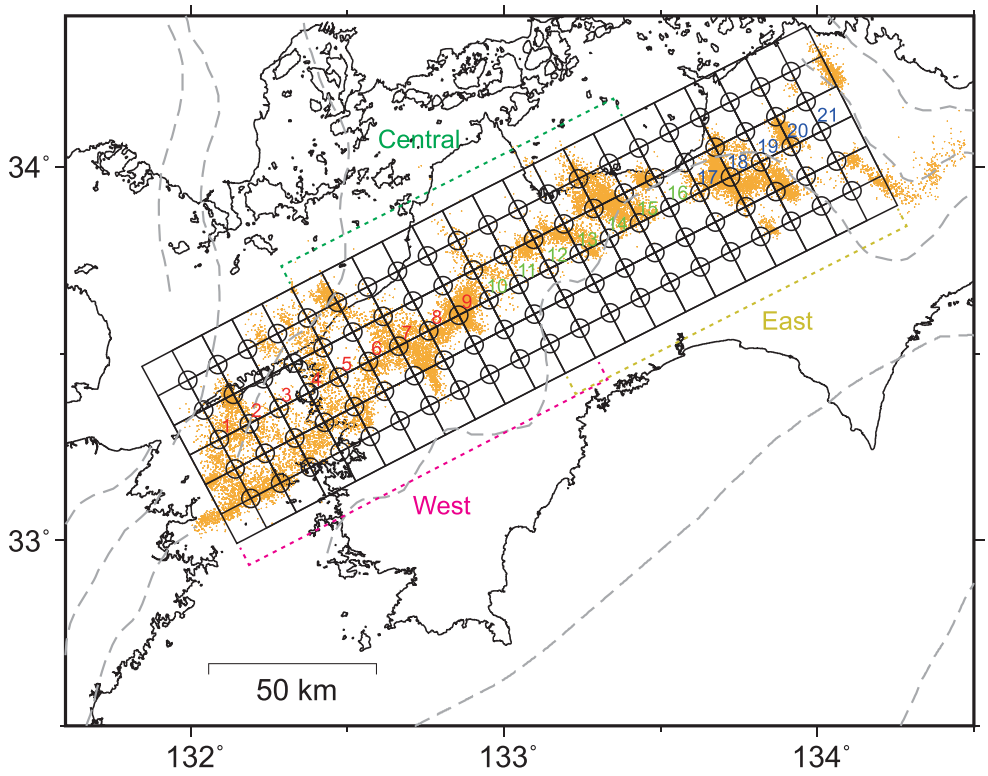

Figure 2. Distribution of the basis functions (rectangles with an open circle in the center) for expressing a slip distribution. The dashed curves denote the plate interface geometry, and the orange dots show the tremor epicenters. West, Central, and East indicate three subregions. The numerals from 1 to 21 close to the open circles represent the number of each knot position of a basis function for Figure 8.

where t_{E}^{i} and t_{N}^{i} denote the tilt changes in the east and north directions, respectively, at the ith station, and N_{sta} represents the number of tilt stations. The superscript T denotes the transpose of a matrix or a vector. The design matrix H consists of

$$\mathrm{H} = \begin{bmatrix} \mathrm{G} \\ \alpha \mathrm{S} \\ \beta \mathrm{Z} \end{bmatrix}, \tag{3}$$

where each element in G represents an elastostatic Green's function for a tilt change at a surface station due to a unit slip distribution on a basis function ($2N_{\mathrm{sta}} \times M$ matrix), S is a Laplacian operator matrix ($M \times M$) for constraining the smoothness of a slip distribution, Z is a matrix ($M \times M$) for constraining slip on the ends of the modeled area to be 0, and α and β, respectively, denote the hyperparameters for controlling the weights of the above two constraints. We apply a nonnegative least squares method (Lawson & Hanson, 1974) to solve the above observation equation with weights by the inverse of the standard deviation of each component of the tilt data. The hyperparameters for these two constraints are determined through minimization of Akaike's Bayesian Information Criterion (ABIC; Akaike, 1980), where the formulation of ABIC by Fukahata et al. (2004) is used.

We define three subregions for smaller SSEs in addition to the modeled region covering the entire ETS zone in Shikoku. A set of tilt offset data for an event period is inverted four times with each one of four modeled regions: (i) Total, (ii) West, (iii) Central, and (iv) East (Figure 2). We select an appropriate slip distribution for each event period as the final slip distribution by a human inspection from four slip models, which are estimated using each of the four modeled regions. For example, Figure 3a shows the final slip distribution for the April 2006 episode (200604) for the West subregion, and Figure 3b shows the distribution for the February 2018 episode (201802) for the Total region. (All four slip distributions with each of the modeled regions for the two SSE episodes are shown in Figures S2 and S3.)

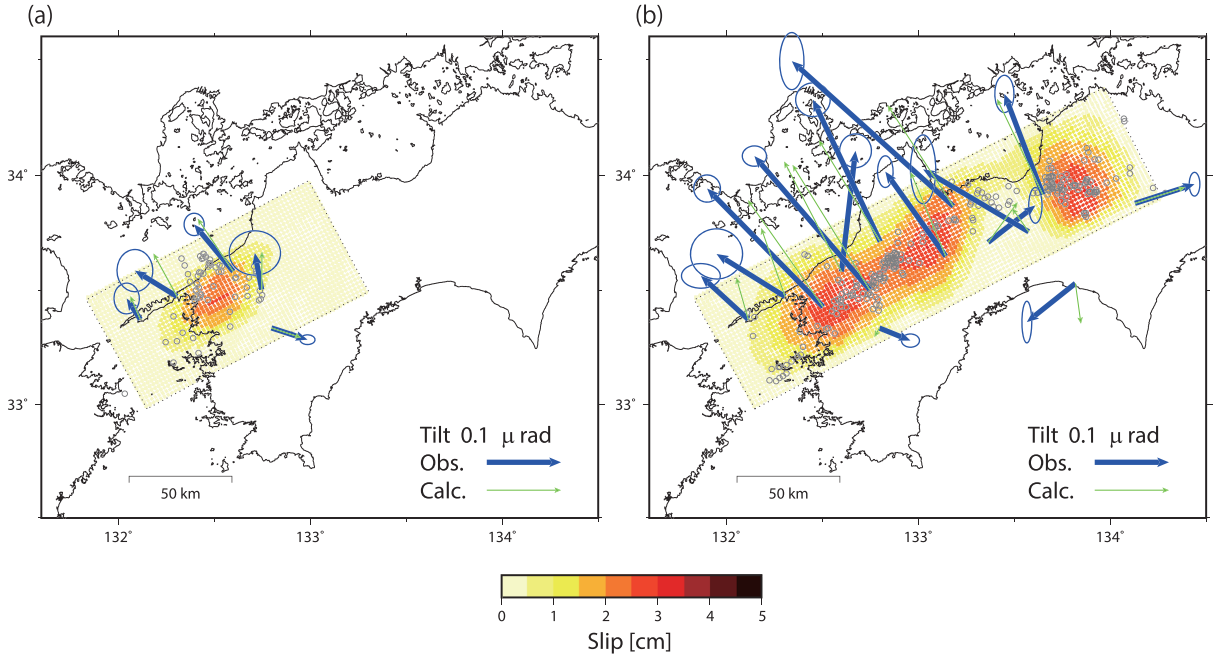

Figure 3. Estimated slip distributions for (a) the April 2006 episode and (b) the February 2018 episode. The blue and green arrows denote the observed and calculated tilt changes, respectively. An error ellipse at each of the observed tilt vector shows a standard deviation. The gray circles indicate the tremor epicenters that occurred during the SSE episode.

Before applying the inversion method to actual observation data, we tested the spatial resolution of a slip distribution based on the current tiltmeter station locations. First, a slip distribution with a checkerboard pattern is given. A set of expected tilt offsets at the station locations is computed. Pseudodata are generated as a Gaussian random noise with a standard deviation of 10^{-8} radians (a typical short-term noise level of the NIED Hi-net tiltmeter data; Hirose & Obara, 2005), 2×10^{-8} radians, or 3×10^{-8} radians is added to each component of the computed tilt offsets. These pseudodata are then inverted to obtain an estimated slip distribution. Figures S4–S7 show the results of the resolution tests for the four modeled regions with the same station distributions as 201802 (Total), 200604 (West), 201412 (Central), and 201811 (East) SSEs, respectively, with each one of the three assumed standard deviations for the random noise. For the cases with the standard deviations of the added noise of $1–2 \times 10^{-8}$ radians, which correspond to most of noise levels of the used data set, slip at a position surrounded by multiple stations is reproduced. In other words, the number of available stations is crucial for the reproduction and the resolution of a slip distribution. For example, in the case with the station locations of the 201812 SSE (Figure S4), slip near the eastern end of the modeled region almost disappears. This is probably because there is just one station close to the given slip patch located near the eastern end. Slip patches at the downdip end in the modeled region is more difficult to be resolved, especially in the central and eastern parts of the ETS zone in Shikoku. From these results, it is said that a slip extension to the strike direction of the Nankai margin can be discussed but a slip extension to the dip direction is more difficult to be observed from the data set used.

4. Results

We estimated a slip distribution for each of the 61 SSE episodes based on the tilt offset data. The estimated slip distributions for all SSEs are shown in Figure S9, and the list of event ID, event time period, seismic moment (M_0), etc. is presented in Table 1.

Figure 4 shows the frequency-magnitude distribution of the short-term SSEs estimated in this study. The moment magnitude (M_w) ranges from 5.7 to 6.4, and the average is 6.0. It is likely that smaller SSEs occur more frequently than larger SSEs (e.g., Wech et al., 2010), but the distribution shows that the number of SSEs smaller than M_w 6.0 decreases as M_w becomes smaller. This indicates that a number of SSEs smaller than $M_w \sim 6.0$ are likely to be undetected. Indeed, for example, an SSE in central Shikoku in September 2017 (M_w 5.7) is reported based on a data analysis with strainmeters and tiltmeters (AIST & NIED, 2018), but this

Table 1
Event Parameters for Short-Term SSEs

Event ID	Start date	End date	Duration (day)	M_0 (Nm)	M_w	Max. slip (cm)
200101	2001/01/04	2001/01/12	8	7.3e+17	5.8	0.8
200108	2001/08/16	2001/08/20	4	1.2e+18	6.0	3.7
200202	2002/02/10	2002/02/18	8	1.6e+18	6.1	2.5
200208	2002/08/06	2002/08/13	7	1.1e+18	6.0	1.8
200304	2003/04/17	2003/04/21	4	8.4e+17	5.9	1.4
200308	2003/08/27	2003/09/04	8	1.4e+18	6.0	5.2
200311	2003/11/07	2003/11/13	6	2.4e+18	6.2	3.2
200311C	2003/11/19	2003/11/25	6	1.3e+18	6.0	1.7
200402	2004/02/10	2004/02/13	3	7.1e+17	5.8	1.2
200404	2004/04/19	2004/04/26	7	1.1e+18	6.0	2.1
200412	2004/12/27	2005/01/01	5	1.2e+18	6.0	2.7
200505	2005/05/12	2005/05/18	6	1.2e+18	6.0	3.8
200510	2005/10/23	2005/10/27	4	5.5e+17	5.8	2.3
200604	2006/04/15	2006/04/20	5	9.3e+17	5.9	2.6
200609	2006/09/08	2006/09/17	9	2.8e+18	6.2	2.0
200611E	2006/11/07	2006/11/11	4	4.6e+17	5.7	0.8
200703	2007/03/13	2007/03/17	4	1.0e+18	5.9	2.6
200709A	2007/08/28	2007/09/03	6	1.1e+18	6.0	0.8
200709B	2007/09/09	2007/09/12	3	6.6e+17	5.8	1.3
200712	2007/12/19	2007/12/25	6	1.7e+18	6.1	2.4
200802E	2008/02/13	2008/02/18	5	5.8e+17	5.8	2.3
200803	2008/03/14	2008/03/18	4	1.0e+18	5.9	3.5
200809	2008/09/27	2008/10/04	7	1.8e+18	6.1	5.3
200810	2008/10/13	2008/10/17	4	8.7e+17	5.9	1.6
200904	2009/04/07	2009/04/15	8	2.2e+18	6.2	3.4
200905C	2009/05/23	2009/05/25	2	4.6e+17	5.7	1.0
200910	2009/10/29	2009/11/10	12	1.5e+18	6.1	2.4
200912C	2009/12/27	2010/01/01	5	1.3e+18	6.0	1.9
201003A	2010/02/28	2010/03/07	7	1.6e+18	6.1	2.3
201003B	2010/03/27	2010/04/02	6	1.9e+18	6.1	2.5
201008	2010/08/13	2010/08/20	7	2.9e+18	6.2	3.5
201011E	2010/11/09	2010/11/11	2	6.0e+17	5.8	1.6
201012	2010/12/09	2010/12/16	7	1.5e+18	6.0	3.0
201101	2011/01/10	2011/01/14	4	8.4e+17	5.9	2.4
201105	2011/05/21	2011/05/24	3	7.1e+17	5.8	1.6
201107	2011/07/02	2011/07/04	2	6.0e+17	5.8	1.4
201108	2011/08/10	2011/08/19	9	1.8e+18	6.1	3.4
201112	2011/12/24	2011/12/28	4	5.7e+17	5.8	1.3
201201	2011/12/31	2012/01/11	11	3.2e+18	6.3	2.5
201205	2012/05/25	2012/06/04	10	1.2e+18	6.0	2.4
201208E	2012/08/04	2012/08/10	6	8.4e+17	5.9	3.6
201211	2012/11/30	2012/12/15	15	4.3e+18	6.4	3.4
201305	2013/05/24	2013/05/28	4	1.3e+18	6.0	2.3
201306	2013/06/02	2013/06/11	9	2.6e+18	6.2	2.8
201311E	2013/11/29	2013/12/04	5	8.9e+17	5.9	2.0
201404E	2014/04/14	2014/04/19	5	8.2e+17	5.9	1.9
201405	2014/05/03	2014/05/22	19	3.1e+18	6.3	3.6

Table 1 *(Continued)*

Event ID	Start date	End date	Duration (day)	M_0 (Nm)	M_w	Max. slip (cm)
201409	2014/09/22	2014/09/25	3	9.3e+17	5.9	2.0
201410	2014/10/17	2014/10/22	5	7.4e+17	5.8	1.6
201412	2014/12/26	2015/01/05	10	1.6e+18	6.1	3.1
201501	2015/01/10	2015/01/12	2	9.0e+17	5.9	1.7
201505	2015/05/28	2015/06/03	6	1.7e+18	6.1	4.0
201509	2015/09/01	2015/09/06	5	1.5e+18	6.1	2.3
201510	2015/10/29	2015/11/07	9	2.3e+18	6.2	3.5
201610	2016/10/24	2016/10/27	3	2.0e+18	6.1	2.8
201703	2017/03/02	2017/03/10	8	2.6e+18	6.2	3.0
201707	2017/07/20	2017/07/25	5	1.3e+18	6.0	2.3
201802	2018/02/21	2018/03/25	32	5.1e+18	6.4	3.0
201810	2018/09/30	2018/10/08	8	2.3e+18	6.2	4.4
201811	2018/10/30	2018/11/03	4	8.8e+17	5.9	1.9
201903	2019/03/02	2019/03/08	6	3.9e+18	6.3	4.6

Note. Dates are formatted as YYYY/MM/DD.

episode is not included in our catalog. This suggests that the SSE catalog constructed in this study is almost complete for M_w larger than 6.0.

This number of events (61) is the total number of short-term SSEs in Shikoku for which rectangular fault models have already been estimated. Hirose and Obara (2010) estimated the spatial and temporal slip evolutions of several short-term SSEs in western Shikoku by applying an NIF technique to tilt time series data. Although their study was the first to estimate a spatial slip distribution for a short-term SSE in southwest Japan, they were unable to obtain a slip distribution for some episodes. One of the reasons that they did not obtain all of the slip distributions is probably that the tilt time series data might be affected by unmodeled disturbances, such as rainfall, and so the data are not appropriate for analysis by their method. Since the inversion method in this study does not require time series data, this method is more robust than that of Hirose and Obara (2010). This contributes the completeness of the obtained catalog of slip distributions of the short-term SSEs in Shikoku.

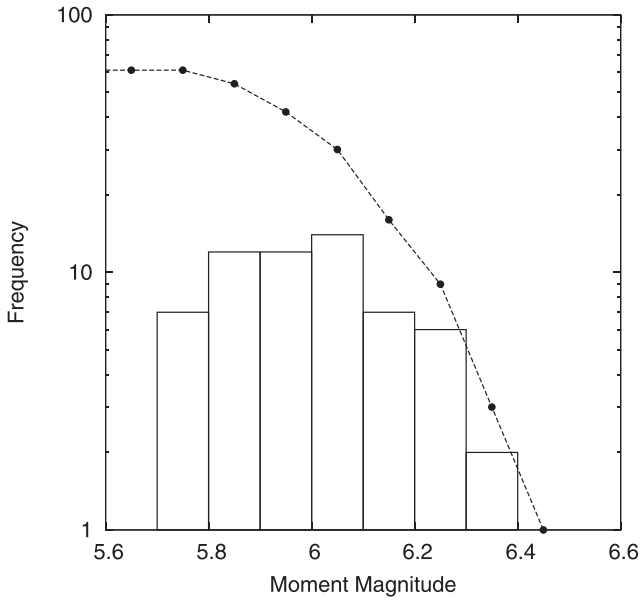

Figure 4. Frequency-magnitude distribution of the short-term SSEs in Shikoku. The histogram shows the number of SSEs that have a moment magnitude in each bin. The solid circles with lines denote the cumulative number of SSEs.

Figure 3 shows slip distributions for two episodes (200604 and 201802) as examples. For the April 2006 episode (200604, Figure 3a), significant tilt changes on the order of 10^{-7} to 10^{-8} radians are recorded at five stations located in the western part of Shikoku, and the slip patch with a maximum slip of 2.6 cm, which corresponds to M_0 9.3 × 10^{17} Nm (M_w 5.9), is estimated. The synthetic tilt changes (green arrows in Figure 3a) roughly explain the observed tilt changes (blue arrows). This solution is comparable to a rectangular fault model in Sekine et al. (2010) and a slip distribution in Hirose and Obara (2010) in terms of location of slip, amount of slip, fault area, and seismic moment. The location of the slip patch correlates well with the epicenters of the tremors that occurred during this episode. For the February 2018 episode (201802, Figure 3b), most of the 14 stations in an area wider than those of the April 2006 episode record large tilt changes greater than 10^{-7} radians. The slip area extends approximately 200 km in Shikoku and has three peaks in the slip distribution. The maximum slip is 3.0 cm. The size of the SSE is estimated to be M_0 5.1 ×10^{18} Nm (M_w 6.4). This is the largest short-term SSE among all of the studied events in 18 years.

Figure 5 shows a spatial and temporal slip distribution for all of the short-term SSEs estimated in this study. The Shikoku area appears to be divided into three segments in terms of short-term SSE activity. We define

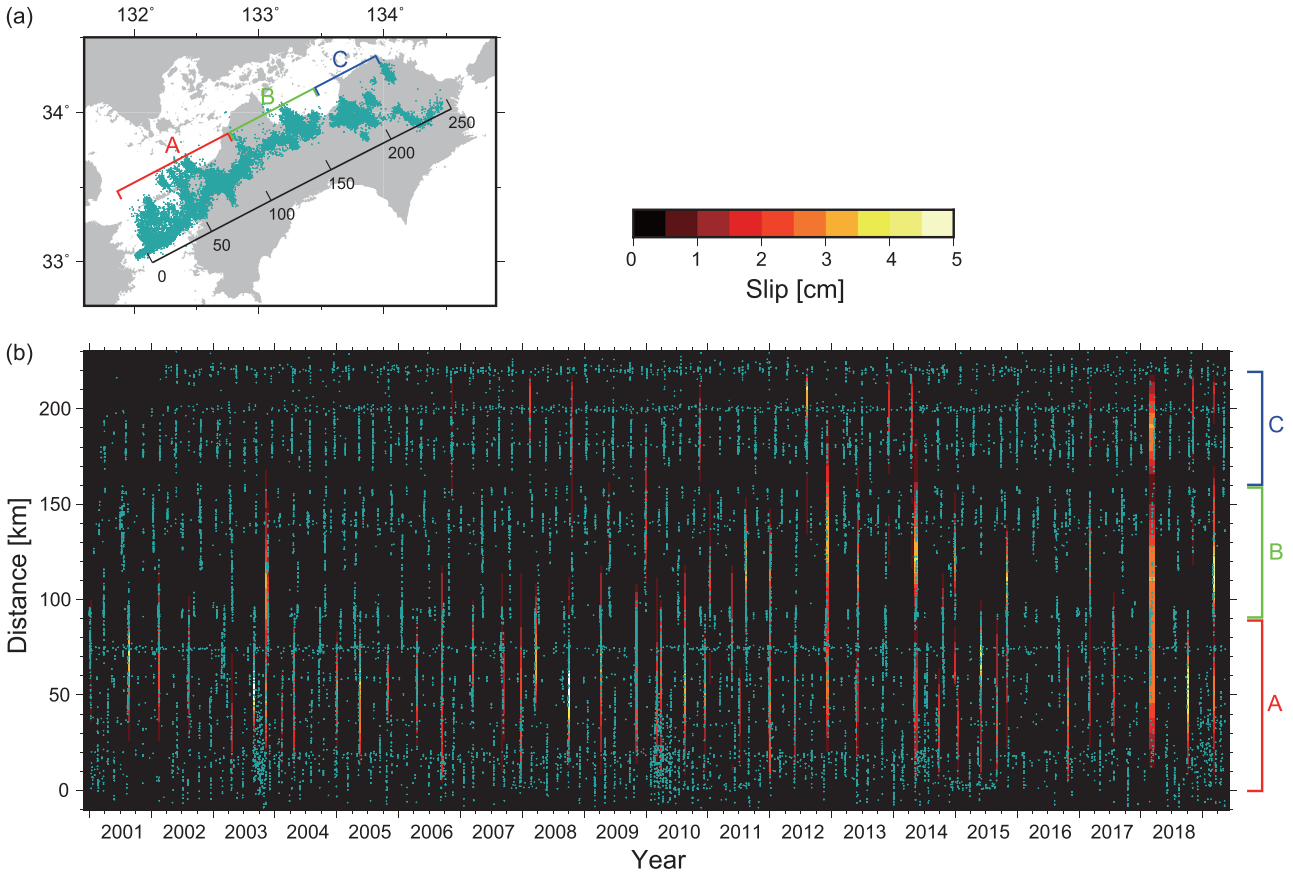

Figure 5. (a) Map of the study area. The distance scale (in kilometers) for (b) is shown. The blue dots represent the tremor epicenters over 18 years. (b) Slip distributions of short-term SSEs in Shikoku projected onto the strike direction as a function of time. A slip distribution of an SSE is denoted as a rectangle, and the amount of slip is color coded. The horizontal range of a rectangle indicates its duration, and the vertical axis indicates the slip position in the distance scale in (a). The blue dots indicate the tremor epicenters.

Segments A (0–90 km), B (90–160 km), and C (160–220 km) based on the SSE slip extents (Figure 5b) and the long-term averaged slip rate distribution (Figure 6). This definition of the segmentation in the short-term SSE source areas is consistent with the tremor activity in Shikoku (Obara, 2010). Among these segments, western Shikoku is the most active segment, where an SSE is detected once every 141 days on average. Before 2011, all of the episodes except for one SSE (200311) occurred within any one of the three segments. However, the number of SSEs in which the slip area extends to multiple segments increases after 2012. This trend is also observed in Figure 7a. We define the length of the slip extent as the length of a slip profile, which is a projection of the spatial slip distribution of an SSE onto the strike direction of the modeled region, where slip larger than 0.5 cm is taken into account. During the study period before around 2010, the length of slip extent scatters almost in the range 50–100 km, whereas in the latter half of the period, several episodes have lengths of slip extents greater than 100 km. Figure 7b shows the seismic moment of the SSEs as a function of time. This also shows a similar trend to the length of slip extent observed in Figure 7a; that is, the number of larger SSEs appears to increase after around 2012.

Only a few episodes having slip areas located on Segment B or C occur before around 2010 (Figure 5). This is probably because the average size of the SSEs in Segment B and C are smaller than those in Segment A and smaller than the detection threshold of the tiltmeter network in these areas. This difference in size is seen in Nishimura et al. (2013). However, because SSEs whose slip area extends to multiple segments have a larger size in moment and slip extent, such an SSE becomes large enough to be detected. In contrast, Nishimura et al. (2013) detected more events in Segment B and C than in this study (Figure S8) with a GNSS network. This suggests the detectability of short-term SSEs is better with the GNSS than the tiltmeters.

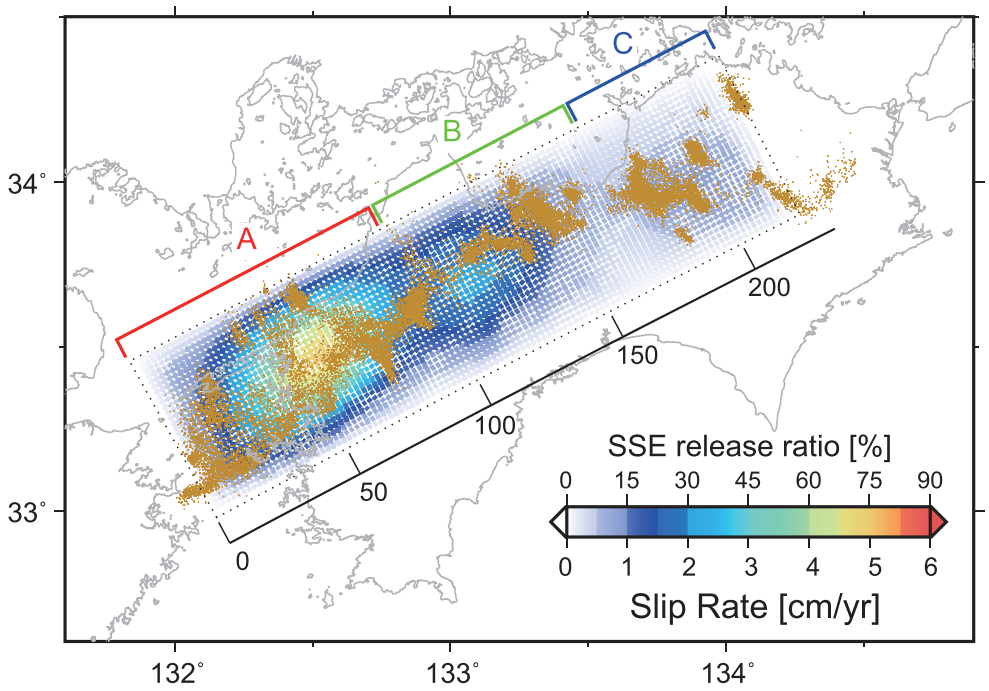

Figure 6. Average slip rate distribution in terms of short-term SSEs over 18 years (2001–2019). The color scale shows the average slip rate. This directly corresponds to the SSE release ratio, which is a ratio of cumulative SSE slip to a plate convergence length for the same period. The orange dots indicate tremor epicenters during the study period. A, B, and C denote the segments defined by the spatial distribution of the slip rate.

Figure 8 shows the cumulative slip history at each knot position, which is located at the center in the dip direction of the modeled region aligned along the strike direction for 18 years in Shikoku. First, we briefly point out the long-term (18 years) average of the slip rate at each position. This rate demonstrates along-strike variation. In Segment A (red curves in Figure 8), the average slip rates are the fastest among the three segments and range from 0.9 to 5.1 cm/year. In Segment B (green curves), the average slip rates are intermediate rates (0.6–2.2 cm/year). In Segment C, the average slip rates are the slowest rates (blue curves, 0.5–0.8 cm/year). In terms of the long-term average slip rate, there are only two knot positions (#5 and #6) where the average slip rate is comparable (~5 cm/year) to the plate convergence rate (~6 cm/year) (Miyazaki & Heki, 2001) in this region. At the other positions, the average slip rate is significantly slower than the plate convergence. Next, we focus on the shorter-term variation in the slip history. The slip history in Segment A is characterized by a cycle of an active period with a higher slip rate associated with a Bungo Channel SSE and an inter-SSE period with a lower slip rate, especially at Knot Positions #1–6 (Figure 8). In Segment B, the slip rate before 2010 is very low but after the 2010–2011 slip appears to accelerate. In Segment C, almost no slip is detected before 2006, and a low, but nearly a constant slip rate (with some fluctuations) is observed thereafter. Note that the long-term averaged slip rate and the shorter-term variation in Segments B and C could be underestimated because of possible undetected SSEs.

5. Discussion

This study enables us to examine the slip history at each position on the plate interface in the ETS zone in Shikoku, which was not discussed in the previous studies (Nishimura et al., 2013; Sekine et al., 2010). This is because our catalog of short-term SSEs in Shikoku contains a spatial slip distribution for each SSE and therefore provides a tool for considering the spatial variation of the slip history on a much smaller spatial scale than the previous studies (e.g., Figure 8).

The slip history at each knot position in the modeled region shows the along-strike variation in the long-term average slip rate and shorter-term fluctuations in the SSE activity (Figure 8). Some of the acceleration phases correspond spatially and temporally to long-term SSEs that occurred in the gap zone between the shallower megathrust earthquake source area and the deeper ETS zone (Figure 1; Takagi et al., 2019). This can also be

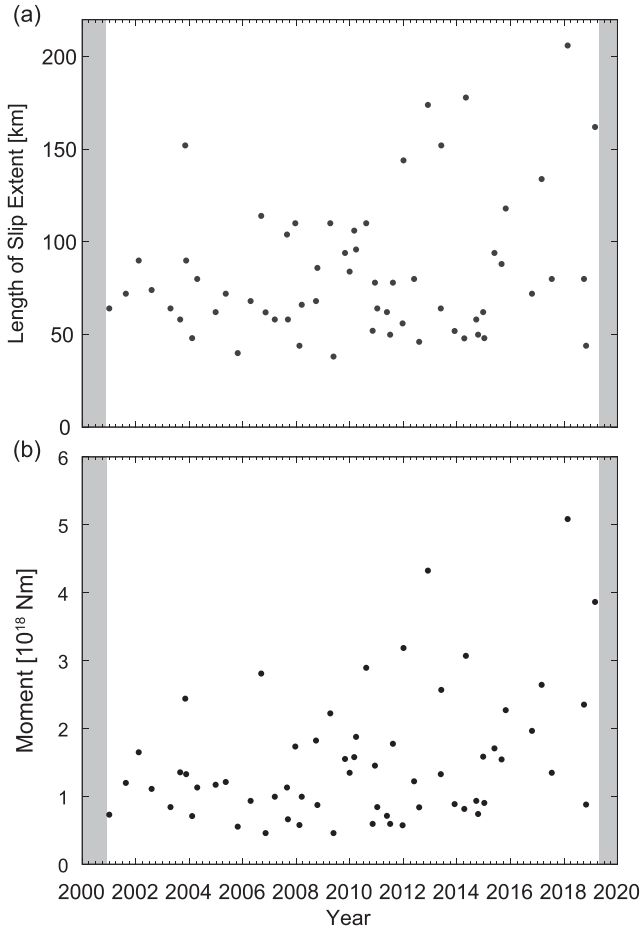

Figure 7. (a) Length of slip extent of the short-term SSEs versus time. (b) Seismic moment of the short-term SSEs versus time. Time periods with gray shading indicate those are not analyzed.

seen in Movie S1. This indicates that the acceleration phases in the short-term SSEs are probably induced by the occurrence of nearby long-term SSEs, as suggested by Hirose and Obara (2005) and Nishimura et al. (2013) for the activation of short-term SSEs in western Shikoku affected by the Bungo Channel SSEs. The slip history in Segment B shows that the slip rate increases after 2010–2011 (green curves in Figure 8). Takagi et al. (2019) found that four long-term SSEs in the gap zone that corresponds to Segment B during the analyzed period of the present study (Event Numbers #11, #18, #20, and #24 in Takagi et al., 2019), and three of the four SSEs occurred after 2010. This indicates that sources of the long-term SSEs in the gap zone are located just updip of the ETS zone, and the long-term SSEs promote the generation of the short-term SSEs in the ETS zone, probably through stress concentration on the ETS zone due to slip on the gap zone. In addition, Takagi et al. (2019) did not detect any SSEs at locations corresponding to Segment C, and the short-term SSE behavior in Segment C shows a nearly constant rate throughout most of the study period (blue curves in Figure 8). This evidence suggests that the short-term SSEs in Segment C keep their regular occurrence behaviors without a disturbance from slip on the adjacent gap zone. This may also support the suggested connection between the short-term SSEs in the ETS zone and the long-term SSEs in the gap zone.

We observe an increase in the number of short-term SSEs with larger slip extent and seismic moment after around 2012 (Figures 5 and 7). Takagi et al. (2016) reported that a change in along-strike tremor migration pattern occurred around 2011. Before 2011, migrations of tremor episodes in western Shikoku terminated at a particular area that corresponds to the segment boundary between A and B in this study (Figures 5 and 6), but in some later episodes tremor activities migrated farther to the east crossing the segment boundary (Takagi et al., 2016). On the other hand, Kono et al. (2020) reported that seismic moment rate inferred from apparent moment of tremors in Shikoku did not change around 2011. Taking these two observations into consideration, a probable scenario is that long-term slip rate in the ETS zone does not change largely as in

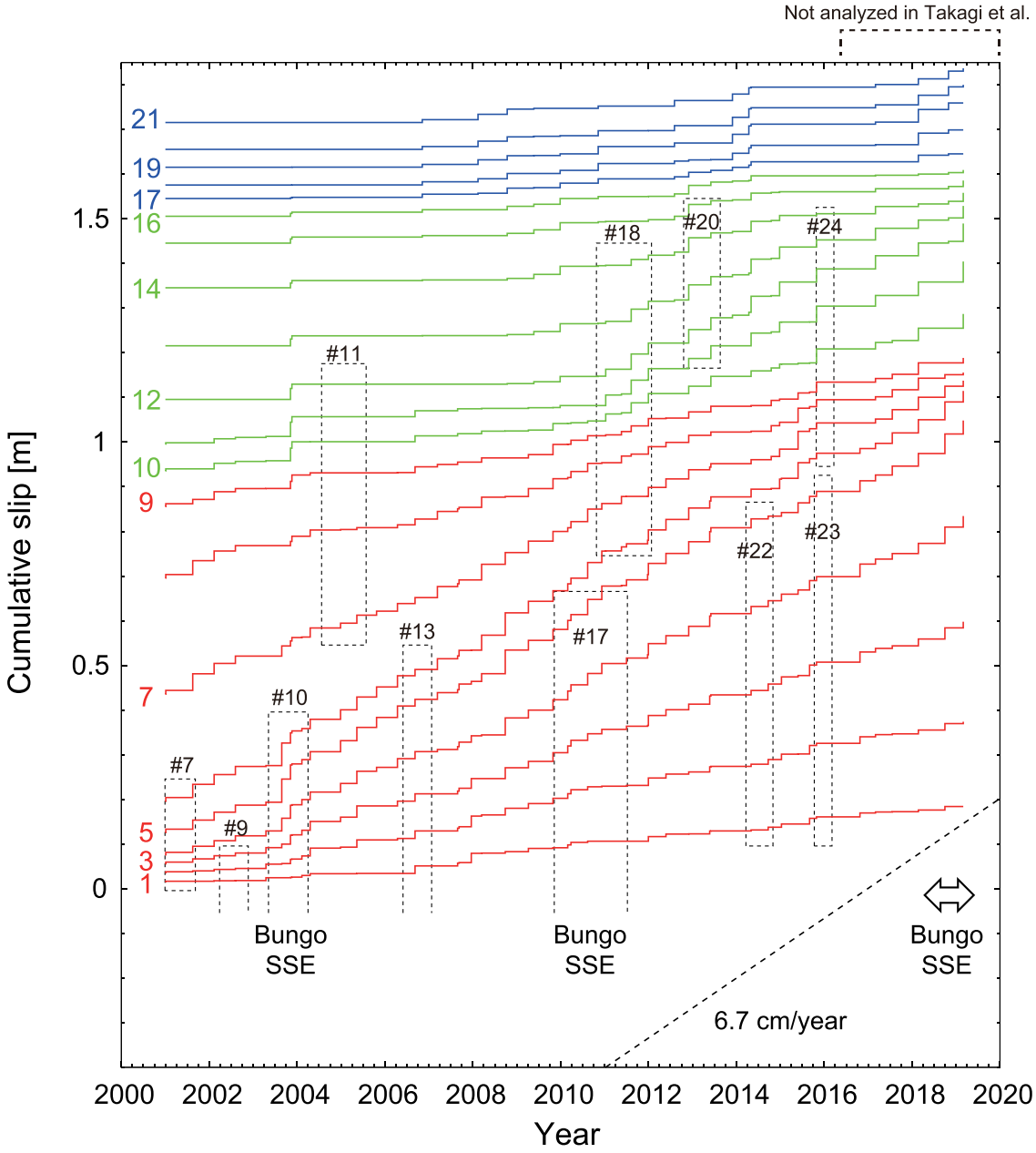

Figure 8. Cumulative slip at each knot position in the modeled region on the plate interface. From bottom to top, cumulative slip histories at each knot from #1 to #21 (the knot positions are indicated in Figure 2). The colors of each trace correspond to the segments shown in Figures 5 and 6. Dashed rectangles show approximate positions and durations of the long-term SSEs (Takagi et al., 2019). Note that each trace is arbitrary shifted in the vertical direction for clarity.

Segment A (Figure 8), but the occurrence of a long-term SSE in the gap zone induces a synchronization of the timing of slip occurrence on the adjacent segments, and then the resultant slip extent and the seismic moment of a connected short-term SSE becomes larger.

Figure 9 shows the cumulative seismic moment released by the short-term SSEs in each segment and in the entire modeled region. The characteristic slip histories for each segment observed in Figure 8 are also shown in this figure. In Segment A, almost constant moment release over two decades appears with some fluctuations. In Segment B, an acceleration in moment release appears to occur around 2010–2011. In Segment C, a nearly constant rate with some fluctuations after approximately 2006 is observed. This along-strike variation in moment release by short-term SSEs is basically in agreement with that estimated based on GNSS displacements (Nishimura et al., 2013) if we compare the moment release for a common time interval, for example,

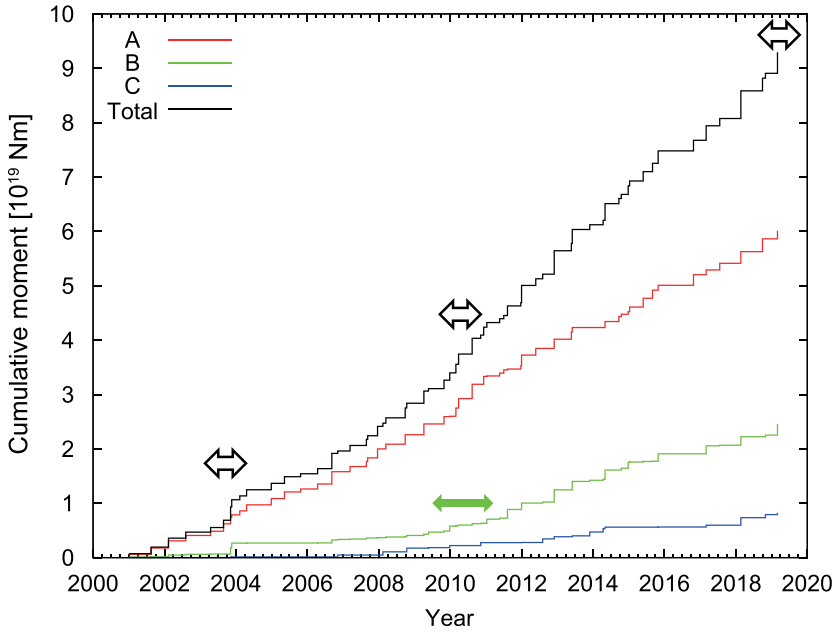

Figure 9. Cumulative seismic moment as a function of time. The red, green, and blue curves show the cumulative seismic moment for Segments A, B, and C, respectively. The black curve denotes the total of the three segments. The open arrows represent time intervals of Bungo Channel long-term SSEs (e.g., Hirose & Obara, 2005; Hirose et al., 2010; Ozawa et al., 2004, 2013).

from 2004 to 2012. The moment release rate in Segment C (blue curve in Figure 9) is much lower than that in Nishimura et al. (2013) ("Eastern Shikoku" in Figure 10 in Nishimura et al., 2013). This difference is probably caused by undetected events in the present study.

In order to discuss the interplate strain budget in the ETS zone, we calculate the average slip rate distribution on the modeled region by dividing the cumulative slip of all of the analyzed SSEs at each position by the studied time period of 18.2 years (Figure 6). The following characteristics are seen in the distribution: (1) There are three peaks in the average slip rate distribution, which correspond to the three segments defined above in the spatial and temporal slip distribution of the SSE slip (Figure 5); (2) the width of the slip zone in the dip direction in Segment A is wider than that in Segment B, which is consistent with the tremor epicenter distribution (e.g., Obara et al., 2010); (3) most of the ETS zone does not release all of the accumulated strain by the relative plate motion, although the maximum slip rate in Segment A in a very small area reaches 5.1 cm/year, similar to the plate convergence rate. Note that this slip rate distribution qualitatively agrees with the cumulative slip distribution estimated using the GNSS displacement data from June 1996 to January 2012 (Nishimura et al., 2013). This supports the validity of the slip rate distribution in the present study.

Recent studies on interplate coupling in southwest Japan exhibit a larger slip-deficit rate on the ETS zone in western Shikoku than in eastern Shikoku (e.g., Nishimura et al., 2018; Noda et al., 2018). Using a block model and onland GNSS and offshore GNSS/Acoustic velocity measurements, Nishimura et al. (2018) estimated that the slip-deficit rate is 30 to 40 mm/year in the westernmost part of the ETS zone in Shikoku and approximately 0 to 20 mm/year in central and eastern Shikoku and decreases monotonically eastward. Noda et al. (2018) also inverted a strain field derived from a similar data set to that in Nishimura et al. (2018) assuming a viscoelastic medium and showed that the slip-deficit rate is 20–40 mm/year in the ETS zone and slightly smaller in eastern Shikoku than rest of the ETS zone. Since both of their data sets are based on secular velocities at observation sites for a time interval without the occurrence of the Bungo Channel long-term SSEs, they do not include displacements due to the long-term SSEs but should include the short-term SSEs displacements. This means that their estimated slip-deficit rate at a position in the ETS zone should be smaller than an actual value in an inter-short-term SSE period. In other words, if the plate interface is fully coupled except for slip during short-term SSEs, the relative plate convergence rate should be equal to the sum of the slip-deficit rate plus the long-term slip rate due to the short-term SSEs. In western Shikoku, the slip-deficit rate is estimated to be approximately 20 to 40 mm/year (Nishimura et al., 2018; Noda et al., 2018)

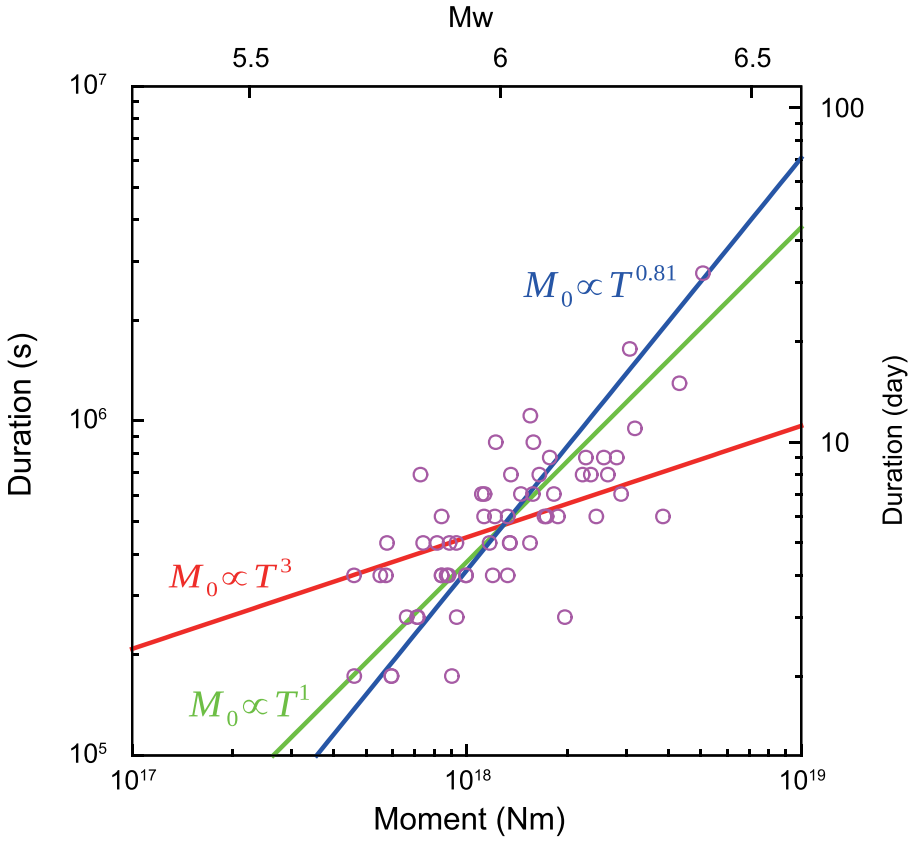

Figure 10. Duration versus seismic moment for the short-term SSEs in Shikoku. Open circles show 61 SSEs analyzed in this study.

and the long-term slip rate ranges from 30 to 50 mm/year in most of the ETS zone (Figure 6). This indicates that the above relationship between the plate convergence rate, the slip-deficit rate, and the slip rate due to the short-term SSEs is approximately satisfied in western Shikoku. This suggests that the plate interface is fully coupled other than for the short-term SSE episodes in the ETS zone in western Shikoku and that the estimated slip deficit could be released by slip events other than short-term SSEs, such as long-term SSEs, or coseismic slip or afterslip of megathrust earthquakes. On the other hand, in eastern Shikoku, since the slip-deficit rate is 0–20 mm/year (Nishimura et al., 2018; Noda et al., 2018) and the slip rate due to short-term SSEs is 0–20 mm/year (Figure 6), the sum of both quantities is 0–40 mm/year, which is much smaller than the plate convergence rate. This suggests that other processes, such as undetected SSEs (short- and/or long-term) and steady creep, may occur in the ETS zone in central and eastern Shikoku.

A key issue for understanding the physics governing slow earthquakes is a scaling relationship between seismic moment M_0 and duration T. Ide et al. (2007) proposed that M_0 of slow earthquakes scales linearly with T, while there are some studies reporting M_0 scales with T^3 like ordinary earthquakes (e.g., Frank & Brodsky, 2019). Since slip distributions for the short-term SSEs in Shikoku are modeled better than previous studies, this study provides us an improved estimation of a set of M_0 of the SSEs, and hence, it is useful for the discussion of the scaling relationship. Using our catalog, we find a relation $M_0 \propto T^{0.811\pm0.093}$ (Figure 10), supporting the scaling relationship $M_0 \propto T$ (Ide et al., 2007). We interpret this as SSEs whose area is bounded by the width of the ETS zone (Gomberg et al., 2016). Since the moment range of our catalog is very limited, however, it is important to extend the moment and duration range of a catalog in order to constrain the scaling relationship.

In order to improve our knowledge of the strain budget and slip behavior in the ETS zone, it is important to obtain a more complete catalog of short-term SSEs. This study is based on tilt offset measurements in which a transient event period is detected by a human inspection. Nishimura et al. (2013) applied a systematic detection method to GNSS displacement data and obtained more estimates of short-term SSEs faults than

those in Sekine et al. (2010). In general, the sensitivity of the tiltmeters to a short-term transient crustal deformation is essentially better than GNSS. For example, a reverse slip on a shallow dipping fault at a depth of approximately 30 km with M_w 6.0 causes a tilt change of approximately 10^{-7} radians and a horizontal displacement of 1 to 2 mm at the surface, according to a simple calculation with formulations by Okada (1992). A typical short-term (approximately a day) noise level of a Hi-net tiltmeter is $\sim 10^{-8}$ radians and the typical accuracy of static daily GNSS positioning is on the order of 1 mm. Comparing these quantities, it is expected that a tiltmeter should detect the deformation of a smaller SSE than GNSS. However, the difference in the spatial station density of both observation networks and a wide variety in the site condition of the borehole tiltmeters, such as responses to atmospheric pressure change and rainfall, may cause the difference in the detectability of the short-term SSEs. To obtain a reliable and more complete catalog of short-term SSEs, one possible method may be a joint analysis of tiltmeters, GNSS, and strainmeters in order to increase the available number of observation data. It is also important to apply a systematic and objective detection method to the data set (e.g., Kimura et al., 2011; Nishimura et al., 2013).

6. Conclusions

The slip distributions of 61 short-term SSEs over 18 years (2001–2019) in Shikoku, southwest Japan, were estimated based on NIED tilt offset data. We found that the size of the detected SSEs ranges from 5.7 to 6.4 in moment magnitude, and the average moment magnitude is 6.0. In terms of the slip history of short-term SSEs, the ETS zone in Shikoku is divided into three segments. Before 2011, all of the episodes except for one SSE occurred within any one of the three segments. However, the number of SSEs having a slip area that extended to multiple segments increased after 2012. This trend also appears in the change in length of the slip extent of the SSEs.

The obtained slip history in the ETS zone shows along-strike variation. In Segment A (western Shikoku), slip accelerations that correspond to the occurrence of the Bungo Channel long-term SSEs are clearly seen. In Segment B (central Shikoku), the slip rate before 2010 was very low, but slip appeared to accelerate after 2010–2011. This acceleration phase corresponds to frequent occurrence of long-term SSEs in the gap zone between the shallower megathrust earthquake rupture zone and the deeper ETS zone. In Segment C (eastern Shikoku), almost no slip was detected before 2006, and a low but nearly a constant slip rate is seen thereafter. This evidence strongly suggests that the short-term SSE activity in the ETS zone is largely affected by the long-term SSEs in the gap zone.

The average slip rate over 18 years suggests that the plate interface is fully coupled during an inter-SSE period in the ETS zone in western Shikoku and that the slip deficit could be released by slip events other than short-term SSEs, such as long-term SSEs, or coseismic slip or afterslip of megathrust earthquakes. On the other hand, in eastern Shikoku, where the slip-deficit rate during an inter-SSE period is smaller than in western Shikoku, steady creep and/or undetected SSEs (short- or long-term) may occur.

Data Availability Statement

The NIED tilt offset data set can be obtained from an NIED repository (https://doi.org/10.17598/nied.0015). The NIED tremor catalog used can be downloaded from the Hi-net web page (http://www.hinet.bosai.go.jp/?LANG=en). The atmospheric pressure and rainfall data can be obtained from Japan Meteorological Agency web page (http://www.data.jma.go.jp/obd/stats/etrn/index.php). The subducting Philippine Sea plate interface geometry is based on Shiomi et al. (2008) and Baba et al. (2006). The computer code for calculating tilt deformation due to dislocation developed by Okada (1992) can be obtained from an NIED web page (http://www.bosai.go.jp/study/application/dc3d/DC3Dhtml_E.html).

Acknowledgments
We would like to thank Hisanori Kimura for providing tilt offset measurements for two SSE episodes and Takanori Matsuzawa and Ryota Takagi for their valuable discussion. We would also like to thank Baptiste Rousset and an anonymous reviewer for their constructive and helpful comments. A feasibility test of a preliminary version of the inversion program was performed in part by Wakako Tamura. This work was supported by JSPS KAKENHI JP16K05542 and JP16H06474. Most of the figures were produced using Generic Mapping Tools (Wessel et al., 2013).

References

AIST, & NIED (2018). Short-term slow slip events in the Tokai area, the Kii Peninsula and the Shikoku District, Japan (from May 2017 to October 2017). *Report of the Coordinating Committee for Earthquake Prediction*, *99*, 243–257.

Akaike, H. (1980). Likelihood and the Bayes procedure. *Bayesian statistics* (pp. 143–166). Valencia: University Press.

Ando, M. (1975). Source mechanisms and tectonic significance of historical earthquakes along the Nankai Trough, Japan. *Tectonophysics*, *27*(2), 119–140. https://doi.org/10.1016/0040-1951(75)90102-X

Baba, T., Cummins, P. R., Hori, T., & Kaneda, Y. (2006). High precision slip distribution of the 1944 Tonankai earthquake inferred from tsunami waveforms: Possible slip on a splay fault. *Tectonophysics*, *426*(1), 119–134. https://doi.org/10.1016/j.tecto.2006.02.015

Frank, W. B., & Brodsky, E. E. (2019). Daily measurement of slow slip from low-frequency earthquakes is consistent with ordinary earthquake scaling. *Science Advances*, *5*(10), eaaw9386. https://doi.org/10.1126/sciadv.aaw9386

Fukahata, Y., Nishitani, A., & Matsu'ura, M. (2004). Geodetic data inversion using ABIC to estimate slip history during one earthquake cycle with viscoelastic slip-response functions. *Geophysical Journal International*, *156*(1), 140–153. https://doi.org/10.1111/j.1365-246X.2004.02122.x

Gomberg, J., Wech, A., Creager, K., Obara, K., & Agnew, D. (2016). Reconsidering earthquake scaling. *Geophysical Research Letters*, *43*, 6243–6251. https://doi.org/10.1002/2016GL069967

Hirose, H., Asano, Y., Obara, K., Kimura, T., Matsuzawa, T., Tanaka, S., & Maeda, T.(2010). Slow earthquakes linked along dip in the Nankai subduction zone. *Science*, *330*(6010), 1502. https://doi.org/10.1126/science.1197102

Hirose, H., Hirahara, K., Kimata, F., Fujii, N., & Miyazaki, S. (1999). A slow thrust slip event following the two 1996 Hyuganada earthquakes beneath the Bungo Channel, southwest Japan. *Geophysical Research Letters*, *26*(21), 3237–3240. https://doi.org/10.1029/1999GL010999

Hirose, H., & Obara, K. (2005). Repeating short- and long-term slow slip events with deep tremor activity around the Bungo channel region, southwest Japan. *Earth, Planets and Space*, *57*(10), 961–972. https://doi.org/10.1186/BF03351875

Hirose, H., & Obara, K. (2010). Recurrence behavior of short-term slow slip and correlated nonvolcanic tremor episodes in western Shikoku, southwest Japan. *Journal of Geophysical Research*, *115*, B00A21. https://doi.org/10.1029/2008JB006050

Ide, S., Beroza, G. C., Shelly, D. R., & Uchide, T. (2007). A scaling law for slow earthquakes. *Nature*, *447*(7140), 76–79. https://doi.org/10.1038/nature05780

Kimura, T., Obara, K., Kimura, H., & Hirose, H. (2011). Automated detection of slow slip events within the Nankai subduction zone. *Geophysical Research Letters*, *38*, L01311. https://doi.org/10.1029/2010GL045899

Kobayashi, A. (2010). A small scale long-term slow slip occurred in the western Shikoku in 2005. *Zisin, 2nd Series*, *63*(2), 97–100. https://doi.org/10.4294/zisin.63.97

Kobayashi, A. (2012). Long-term slow slip event around Kochi City from 1977 to 1980. *Zisin, 2nd Series*, *64*(2), 63–73. https://doi.org/10.4294/zisin.64.63

Kobayashi, A. (2017). Objective detection of long-term slow slip events along the Nankai Trough using GNSS data (1996–2016). *Earth, Planets and Space*, *69*(1), 171. https://doi.org/10.1186/s40623-017-0755-7

Kono, Y., Nakamoto, K., & Hiramatsu, Y. (2020). Temporal variation in seismic moment release rate of slow slips inferred from deep low-frequency tremors in the Nankai subduction zone. *Earth, Planets and Space*, *72*(1), 12. https://doi.org/10.1186/s40623-020-1142-3

Lawson, C. L., & Hanson, R. J. (1974). *Solving least squares problems*. Englewood Cliffs, NJ: Prentice-Hall.

Maeda, T., & Obara, K. (2009). Spatiotemporal distribution of seismic energy radiation from low-frequency tremor in western Shikoku, Japan. *Journal of Geophysical Research*, *114*, B00A09. https://doi.org/10.1029/2008JB006043

Mazzotti, S., & Adams, J. (2004). Variability of near-term probability for the next great earthquake on the Cascadia subduction zone. *Bulletin of the Seismological Society of America*, *94*(5), 1954–1959. https://doi.org/10.1785/012004032

Miyazaki, S., & Heki, K. (2001). Crustal velocity field of southwest Japan: Subduction and arc-arc collision. *Journal of Geophysical Research*, *106*(B3), 4305–4326. https://doi.org/10.1029/2000JB900312

NIED (2012). Short-term slow slip events with non-volcanic tremors in southwest Japan (November, 2011–April, 2012). *Report of the Coordinating Committee for Earthquake Prediction*, *88*, 400–404.

Nishimura, T., Matsuzawa, T., & Obara, K. (2013). Detection of short-term slow slip events along the Nankai Trough, southwest Japan, using GNSS data. *Journal of Geophysical Research: Solid Earth*, *118*, 3112–3125. https://doi.org/10.1002/jgrb.50222

Nishimura, T., Yokota, Y., Tadokoro, K., & Ochi, T. (2018). Strain partitioning and interplate coupling along the northern margin of the Philippine Sea plate, estimated from Global Navigation Satellite System and Global Positioning System-Acoustic data. *Geosphere*, *14*(2), 535–551. https://doi.org/10.1130/GES01529.1

Noda, A., Saito, T., & Fukuyama, E. (2018). Slip-deficit rate distribution along the Nankai Trough, Southwest Japan, with elastic lithosphere and viscoelastic asthenosphere. *Journal of Geophysical Research: Solid Earth*, *123*, 8125–8142. https://doi.org/10.1029/2018JB01551

Obara, K. (2002). Nonvolcanic deep tremor associated with subduction in southwest Japan. *Science*, *296*(5573), 1679–1681. https://doi.org/10.1126/science.1070378

Obara, K. (2010). Phenomenology of deep slow earthquake family in southwest Japan: Spatiotemporal characteristics and segmentation. *Journal of Geophysical Research*, *115*, B00A25. https://doi.org/10.1029/2008JB006048

Obara, K., Hirose, H., Yamamizu, F., & Kasahara, K. (2004). Episodic slow slip events accompanied by non-volcanic tremors in southwest Japan subduction zone. *Geophysical Research Letters*, *31*, L23602. https://doi.org/10.1029/2004GL020848

Obara, K., Kasahara, K., Hori, S., & Okada, Y. (2005). A densely distributed high-sensitivity seismograph network in Japan:Hi-net by National Research Institute for Earth Science and DisasterPrevention. *Review of Scientific Instruments*, *76*(2), 21301. https://doi.org/10.1063/1.1854197

Obara, K., & Kato, A. (2016). Connecting slow earthquakes to huge earthquakes. *Science*, *353*(6296), 253–257. https://doi.org/10.1126/science.aaf1512

Obara, K., Tanaka, S., Maeda, T., & Matsuzawa, T. (2010). Depth-dependent activity of non-volcanic tremor in southwest Japan. *Geophysical Research Letters*, *37*, L13306. https://doi.org/10.1029/2010GL043679

Okada, Y. (1992). Internal deformation due to shear and tensile faults in a half-space. *Bulletin of the Seismological Society of America*, *82*(2), 1018–1040.

Okada, Y., Kasahara, K., Hori, S., Obara, K., Sekiguchi, S., Fujiwara, H., & Yamamoto, A. (2004). Recent progress of seismic observation networks in Japan –Hi-net, F-net, K-NET and KiK-net–. *Earth, Planets and Space*, *56*(8), xv–xxviii. https://doi.org/10.1186/BF03353076

Ozawa, S., Hatanaka, Y., Kaidzu, M., Murakami, M., Imakiire, T., & Ishigaki, Y. (2004). Aseismic slip and low-frequency earthquakes in the Bungo channel, southwestern Japan. *Geophysical Research Letters*, *31*, L07609. https://doi.org/10.1029/2003GL019381

Ozawa, S., Yarai, H., Imakiire, T., & Tobita, M. (2013). Spatial and temporal evolution of the long-term slow slip in the Bungo Channel, Japan. *Earth, Planets and Space*, *65*(2), 67–73. https://doi.org/10.5047/eps.2012.06.009

Rogers, G., & Dragert, H. (2003). Episodic tremor and slip on the Cascadia subduction zone: The chatter of silent slip. *Science*, *300*(5627), 1942–1943. https://doi.org/10.1126/science.1084783

Sagiya, T., & Thatcher, W. (1999). Coseismic slip resolution along a plate boundary megathrust: The Nankai Trough, southwest Japan. *Journal of Geophysical Research*, *104*(B1), 1111–1129. https://doi.org/10.1029/98JB02644

Segall, P., & Matthews, M. (1997). Time dependent inversion of geodetic data. *Journal of Geophysical Research*, *102*(B10), 22,391–22,409. https://doi.org/10.1029/97JB01795

Sekine, S., Hirose, H., & Obara, K. (2010). Along-strike variations in short-term slow slip events in the southwest Japan subduction zone. *Journal of Geophysical Research*, *115*, B00A27. https://doi.org/10.1029/2008JB006059

Shiomi, K., Matsubara, M., Ito, Y., & Obara, K. (2008). Simple relationship between seismic activity along Philippine Sea slab and geometry of oceanic Moho beneath southwest Japan. *Geophysical Journal International*, *173*, 1018–1029. https://doi.org/10.1111/j.1365-246X.2008.03786.x

Takagi, R., Obara, K., & Maeda, T. (2016). Slow slip event within a gap between tremor and locked zones in the Nankai subduction zone. *Geophysical Research Letters*, *43*, 1066–1074. https://doi.org/10.1002/2015GL066987

Takagi, R., Uchida, N., & Obara, K. (2019). Along-strike variation and migration of long-term slow slip events in the western Nankai subduction zone, Japan. *Journal of Geophysical Research: Solid Earth*, *124*, 3853–3880. https://doi.org/10.1029/2018JB016738

Wech, A. G., Creager, K. C., Houston, H., & Vidale, J. E. (2010). An earthquake-like magnitude-frequency distribution of slow slip in northern Cascadia. *Geophysical Research Letters*, *37*, L22310. https://doi.org/10.1029/2010GL044881

Wessel, P., Smith, W. H. F., Scharroo, R., Luis, J., & Wobbe, F. (2013). Generic Mapping Tools: Improved version released. *Eos, Transactions American Geophysical Union*, *94*(45), 409–410. https://doi.org/10.1002/2013EO450001

Yagi, Y., Kikuchi, M., Yoshida, S., & Yamanaka, Y. (1998). Source process of the Hyuga-nada earthquake of April 1, 1968 (M_jma 7.5) and its relationship to the subsequent seismicity. *Zisin, 2nd Series*, *51*(1), 139–148. https://doi.org/10.4294/zisin1948.51.1139

Yarai, H., & Ozawa, S. (2013). Quasi-periodic slow slip events in the afterslip area of the 1996 Hyuga-nada earthquakes, Japan. *Journal of Geophysical Research: Solid Earth*, *118*, 2512–2527. https://doi.org/10.1002/jgrb.50161